19th Brazilian Congress of Thermal Sciences and Engineering
November 06th-10th, 2022, Bento Gonçalves - RS - Brazil

ENC-2022-0503
MODELING AND SIMULATION OF INTERNAL CONTROL VALVE (ICV) CALCIUM CARBONATE SCALE FORMATION

Vinicius Gustavo Poletto
Marina Elizabeth Mazuroski
Matheus Rohrich Martins
Fernando Cesar De Lai
Silvio Luiz de Mello Junqueira
Research Center for Rheology and Non-Newtonian Fluid (CERNN) | Federal University of Technology – Parana (UTFPR)
vpoletto@utfpr.edu.br
marina.mazuroski@gmail.com
matmar@alunos.utfpr.edu.br
fernandodelai@utfpr.edu.br
silvio@utfpr.edu.br

Bruno Barbosa de Castro
Mateus Palharini Schwalbert
André Leibsohn Martins
Paulo Guilherme Oliveira de Oliveira
Petróleo Brasileiro S. A. | Petrobrás
bbcastro@petrobras.com.br
mateusps@petrobras.com.br
aleibsohn@petrobras.com.br
pauloguilherme@petrobras.com.br

Abstract. *Modern open-hole full-electric intelligent completion systems, designed to reduce cost and maximize oil output, do not always provide inhibition injection lines for scale control in downhole equipment. The oil industry has reported calcium carbonate scaling in downhole Internal Control Valves (ICV). In fact, the chemical synthesis reaction depends on the concentration of dissolved carbon dioxide. Local pressure drops imposed by valve's ports, for instance, dislocate the chemical equilibrium and trigger the formation of tiny crystals. Besides eventually adhering to the valve and building the scale that obstructs the flow, crystals also impose additional pressure drops. Furthermore, scales deposits can damage the valves' key actuation features, leaving them inoperative and permanently stuck. Traditionally, scale prediction relies on thermodynamic and kinetic analysis, ignoring the influence of fluid dynamics on precipitated crystals and valve geometry. This paper details a Euler-Lagrange approach for modeling the liquid-solid turbulent flow with adhesion to simulate of scale formation in ICVs. Numerical simulation is performed through the Finite Volume method coupled with the Discrete Element Method (CFD-DEM). Results concern the accumulated mass in specific parts of the equipment (fouling hotspots) and the transient pressure uptrend due to flow blockage. The particles represent precipitated crystals in the bulk and adhere to the walls under the action of adhesive forces. The methodology and results presented are helpful for valve qualification in terms of scale formation potential and reliability of valve actuation mechanism.*

Keywords: *Scale Formation, Calcium Carbonate, Internal Control Valve (ICV), Valve Cycling, CFD-DEM*

1. INTRODUCTION

The Brazilian pre-salt reservoirs have shown inorganic scale issues with very low water cut measures. Calcium carbonate scale has been observed even at the beginning of the well lifespan, which indicates the potential of having flow assurance problems (Ferreira et al., 2020). On top of that, modern multiple-zones completion systems use remote-actuated valves to control the production flow rate in each zone (Schnitzler et al., 2021). As pointed out by numerical results (Poletto et al., 2020), the valve itself is scale target due to geometry of the flow ports. Results in terms of the

velocity and pressure obtained for sliding-sleeve valves by Mores et al. (2020) indicate a local and intense pressure drop in the adjacency of the choke. Cosmos et al. (2022) discusses the possibility of displacing chemical equilibria due to carbon dioxide dissolution and, therefore, triggering the precipitation of calcium carbonate. The valve itself eventually washes away the tiny precipitated crystals due to the high flow rate and turbulence dissipation in the flow, also demonstrated by Mores et al. (2020). However, thermodynamic simulation using the MultiScale indicate that reservoir conditions are scale prone, with the probability of forming new crystals increasing as temperature and pressure decreases. In fact, the fluid flow transports already-precipitated crystals, born in formation perforations for instance, to the adjacency of the flow ports (choke). Crystals get closes to each other, building agglomerates that eventually deposits on the walls of the valve. There is also the possibility of growing scale from the wall following a heterogenous nucleation process that depends on the surface hydrophobic characteristics (Cheong et al., 2013) and roughness (Al-Anezi et al., 2008). Usually, experimental testing to assess surface-nucleated scale employs brine as mixture, neglecting the oil phase. In fact, the oil phase plays an important role into the thermodynamic equilibrium (Silva et al., 2018). Moreover, the main aspect of the water-oil liquid-liquid turbulent flow under production flow rates is the dispersion of water droplets into a continuous oil phase (Kokal, 2005) and (Morgan et al., 2019). Under such hypothesis, crystals precipitate within the droplets, constituting a bulk nucleation and corroborating the fact that the valve flow port concentrates all the crystals close together.

Issues regarding scale deposition, or fouling, arise mainly because deposits may increase the pressure drop of the production system, constituting a flow assurance problem. In fact, a local deposition on a valve choke would lead to relevant production losses. Acidification sometimes is necessary to help reestablish the operational pressure of the valve, requiring expensive workover works. Scale deposits may also damage movable parts and eventually let valves stuck permanently in the open, or close, position. Scale would deposit in tiny gaps of the actuation mechanism, building wedges and shims that prevent the movement. The driving system also would require unavailable power to wipe out the deposits and set the valve free. In fact, inorganic scale consists of a flow assurance problem both because of the flow obstruction and the deposition in sensitive movable parts, questioning the reliability of the intelligent completion system. Furthermore, valves may be vulnerable in modern cableless completion systems as there is no chemical inhibitors injections lines available in deeper production zones.

The present paper proposes the application of numerical simulation to assess the effects of inorganic scale in completion valves concerning. The scale formation applies a hybrid Euler-Lagrange approach to model the liquid-solid turbulent flow applying the Finite Volume Method coupled to the Discrete Element Method (CFD-DEM). The main inputs are fluid properties, flow rate, solid injection rate and particle diameter, while the main results are the tendency of pressure increase and the accumulated mass inside the valve. Experimental results obtained by Dynamic Tube Blocking Testing (DTB) and large-scale flow loop with a ssv mock up are reproduced to evaluate the robustness of the method.

2. CFD-DEM FORMULATION FOR SCALE FORMATION

The CFD-DEM modelling solves fluid-solid multiphase flows with the Euler-Lagrange approach, using separate formulations for each phase. The fluid phase is modelled as a continuous flow and solved by using Computational Fluid Dynamics (CFD) techniques. The solid phase is considered composed of discrete, non-deformable spheres, treated by the Dicrete Elements Method (DEM) (Cundall and Strack, 1979). The four-way coupling between the approaches allows for fluid-particle and particle-particle interaction. In the context of scale formation in downhole equipment, the CFD-DEM contemplates already precipitated calcium carbonate crystals as the solid phase, excepting the nucleation and growth stages of crystal formation. The scaling phenomenon is established through the formation and breakage of salt agglomerates, as well as the adhesion and detachment of solids from surfaces. The continuous flow is formulated with average properties of the fluid, and the resulting forces from the interaction with the solid phase are implemented through mathematical expressions. The CFD-DEM modelling is advantageous as it allows for the simulation of a significant number of particles and in-depth analysis of the particles' trajectory.

Among the CFD techniques for the solution of multiphase flows, the Dense Discrete Phase Model (DDPM) by Popoff and Braun (2007) is suited for both dense and dispersed flows. The solid phase presence in the fluid flow is incorporated through adjustment of the mass and momentum balance equations in Equations (1) and (2), respectively.

$$\frac{\partial \alpha_\beta \rho_\beta}{\partial t} + \nabla \cdot \left(\alpha_\beta \rho_\beta \boldsymbol{u}_\beta \right) = 0 \tag{1}$$

$$\begin{aligned} &\frac{\partial \left(\alpha_\beta \rho_\beta \boldsymbol{u}_\beta \right)}{Dt} + \nabla \cdot \left(\alpha_\beta \rho_\beta \boldsymbol{u}_\beta \boldsymbol{u}_\beta \right) = -\alpha_\beta \nabla P + \\ &+ \nabla \cdot \left(\alpha_\beta \mu_\beta \left(\nabla \boldsymbol{u}_\beta + \nabla \boldsymbol{u}_\beta^T \right) \right) + \alpha_\beta \rho_\beta \mathbf{g} + \mathbf{F}_{p\beta} \end{aligned} \tag{2}$$

where ρ_β [kg/m³] is the fluid density, t [s] is the time, $\mathbf{u}_\beta$ [m/s] is the fluid velocity vector, P [Pa] is the pressure, μ_β [Pa.s] is the fluid viscosity and $\mathbf{g}$ [m/s²] is the gravity acceleration vector. Phase interaction is computed by the fluid volumetric fraction α_β [-] and the phase coupling term $\mathbf{F}_{p\beta}$ [N/m³].

Flow turbulence is implemented with the k-ε realizable model (Shih et al., 1995), which shows to be advantageous to the standard k-ε model (Launder and Spalding, 1972) in solving complex flows. Balance equations for the turbulent kinetic energy k [m²/s²] and the turbulent dissipation ε [m²/s³] are given by Equations (3) and (4), respectively.

$$\frac{\partial(\rho k)}{\partial t}+\frac{\partial(\rho k u_i)}{\partial x_i}=\frac{\partial}{\partial x_i}\left[\left(\mu+\frac{\mu_t}{\sigma_k}\right)\frac{\partial k}{\partial x_i}\right]+ \\ +G_k+G_b-\rho\varepsilon-Y_M+S_k \tag{3}$$

$$\frac{\partial(\rho\varepsilon)}{\partial t}+\frac{\partial(\rho\varepsilon u_i)}{\partial x_i}=\frac{\partial}{\partial x_i}\left[\left(\mu+\frac{\mu_t}{\sigma_\varepsilon}\right)\frac{\partial \varepsilon}{\partial x_i}\right]+ \\ +\rho C_1 S\varepsilon-\rho C_2\frac{\varepsilon^2}{k+\sqrt{\nu\varepsilon}}+C_{1\varepsilon}\frac{\varepsilon}{k}C_{3\varepsilon}G_b+S_\varepsilon \tag{4}$$

where u_i [m/s] is the velocity in each direction, μ_t [Pa.s] the turbulent viscosity, σ_k and σ_ε [-] the turbulent Prandtl number for k and ε, respectively. G_k [kg/(m.s³)] is the turbulent kinetic energy generated from gradients of velocity and G_b [kg/(m.s³)] is the turbulent kinetic energy generated from buoyancy. Y_M [kg/(m.s³)] is the contribution from dilatation in turbulent compressible flows, S_k and S_ε [kg/(m.s³)] are source terms and $C_{1\varepsilon}$ and C_2 [-] are constants. Finally, C_1 and S are given by Equations (5), (6) and (7):

$$C_1=max\left(0{,}43;\frac{\eta}{\eta+5}\right) \tag{5}$$

$$\eta=\frac{k}{\varepsilon}\sqrt{2S_{ij}S_{ij}} \tag{6}$$

$$S\equiv\sqrt{2S_{ij}S_{ij}} \tag{7}$$

The trajectory of particles, denoted by the index j, is individually determined by accounting for all interaction forces between phases using Newton's Second Law. The particle velocity vector $\mathbf{u}_{p[j]}$ [m/s] is calculated from Equation (8), from which the particle position $\mathbf{x}_{p[j]}$ [m] is obtained with Equation (9). The particle rotation $\boldsymbol{\omega}_{p[j]}$ [s^{-1}] and the torques acting upon it are calculated with Equation (10):

$$m_{p[j]}\frac{d\boldsymbol{u}_{p[j]}}{dt}=\mathbf{F}_{D[j]}+\mathbf{F}_{G[j]}+ \\ +\mathbf{F}_{PG[j]}+\mathbf{F}_{VM[j]}+\mathbf{F}_{SL[j]}+\mathbf{F}_{C[j]} \tag{8}$$

$$\frac{d\mathbf{x}_{p[j]}}{dt}=\boldsymbol{u}_{p[j]} \tag{9}$$

$$I_{p[j]}\frac{d\boldsymbol{\omega}_{p[j]}}{dt}=\mathbf{T}_{D[j]}+\mathbf{T}_{C[j]} \tag{10}$$

where $m_{p[j]}$ [kg] is the particle mass and $I_{p[j]}$ [kg.m²] is the particle moment of inertia. The forces balance in Equation (8) considers the drag force $\mathbf{F}_{D[j]}$ [N] (Peker et al., 2008), the gravity force $\mathbf{F}_{G[j]}$ [N], the pressure gradient force $\mathbf{F}_{PG[j]}$ [N] (Anderson and Jackson, 1967), the virtual mass force $\mathbf{F}_{VM[j]}$ [N] (Odar and Hamilton, 1964), the Saffman lift force $\mathbf{F}_{SL[j]}$ [N] (Saffman, 1965) and the contact force $\mathbf{F}_{C[j]}$ [N]. The torques balance considers the drag torque $\mathbf{T}_{D[j]}$ [N] and the contact torque $\mathbf{T}_{C[j]}$ [N]. The result of each force term is dependent on experimental or analytical parameters. For the drag force, Morsi and Alexander (1972) provide the drag coefficient for spherical particles. Information on the calculation of the other forces is described by Poletto et al. (2020). Depending on the magnitude of the particles and the fluid flow conditions, additional forces and torques can be included, such as Brownian movement force or magnetic forces.

The contact force and torque are a result of the particle interaction with surfaces or another particle, and are calculated by the DEM. In this model, the contact force consists of collision, friction and adhesion components. The collision is obtained from particle deformation, which is measured by the overlap δ_{ij} [m] during a contact, following the linear hysteresis model (Walton and Braun, 1986). The constant adhesive force model (Marshall and Li, 2014) is responsible for the adhesion, where a constant value of the magnitude of adhesive force $\mathbf{F}_{adh[j]}$ [N] is imposed between two bodies within a predetermined range δ_{adh} [m], as stated by Equation (11):

$$F_{adh[j]} = \begin{cases} 0 & \text{for } \delta_{[ij]} \le \delta_{adh} \\ f_{adh}\, g \min(m_{[i]}, m_{[j]}) & \text{for } \delta_{[ij]} > \delta_{adh} \end{cases} \tag{11}$$

where f_{adh} [-] is a proportionality constant for the adhesive force magnitude and $m_{[i]}$ and $m_{[j]}$ [kg] are the mass of particles i and j, respectively.

3. CFD-DEM VERIFICATION RESULTS: DTB

The experimental test Dynamic Tube Blocking (DTB) is commonly used for the scaling process study and the evaluation of inhibitors efficiency. The DTB representative scheme is displayed in Figure 1. Two ionic solutions are pre-heated and pumped into a capillary duct, where a supersaturated mixture prone to crystal formation is produced. Scale formation is measured by the pressure differential, where an exponential increase is usually observed, as indicated by Figure 2. Due to the small order of magnitude of particles generated during the nucleation stage of crystal formation, pressure sensitivity to the scale process is mainly bound to the adhesion of larger crystals on the walls, causing pipe diameter reduction. The simulation of scaling on the DTB test is advantageous for the geometry simplicity, and can be used to verify the CFD-DEM model capabilities through comparison with the experimental results. Furthermore, it can aid in the process of numerical parameters calibration for the prediction of scale in real downhole conditions.

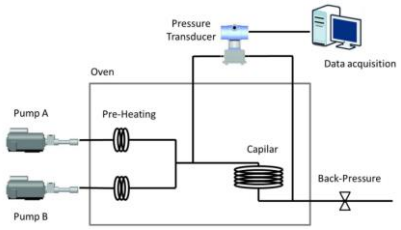

Figure 1. Dynamic Tube Blocking (DTB) test representative scheme. (Santos et al., 2017).

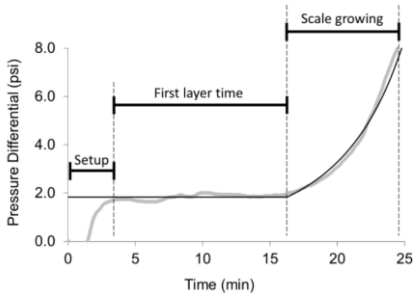

Figure 2. Usual pressure differential response from the Dynamic Tube Blocking test. Adapted from Santos et al. (2017).

The geometry and parameters used in the DTB test simulation were determined from the experimental apparatus and results from Santos et al. (2017). Two cases from the study were reproduced, with parameters listed in Table 1. The geometry consists of a cylindrical pipe with a diameter of 0.5 mm, forming a spiral shape with 100 nm of diameter. Figure 3 displays the geometry and the scale formation at t=30 s of case I. Particles agglomerates can be observed in several parts of the duct, mostly concentrated on the outside are of the spiral due to the inertial centrifugal force.

The CFD-DEM model entails the individual solution of every particle in the domain, which means that the computational cost increases significantly with the number of simulated particles. Therefore, a convenient approach for evaluation of the accuracy of the simulation results is by extrapolating the pressure differential obtained and comparing them to the experimental curves. The extrapolation of the cases I and II is done considering the results for a simulated time of t=27 and 21 s, respectively. Parameters A [-] and B [-] in the function $f(x)=Ax^{Bx}$ were fitted for each test, from which the pressure value was estimated for t=350 s in the extrapolation of case I and t=380 s in case II. Figure 4 displays the comparison between experimental and extrapolated pressure curves for case I, while Figure 5 shows the comparison for case II. The extrapolations displayed excellent agreement to the experimental curves, with R^2=0.97 for

both fits. The results indicate great potential for the predicament of scale formation and behavior using the CFD-DEM model, providing results with similar tendencies to the experimental results even with a few seconds of simulation.

Table 1 – Numerical parameters for the reproduction of experimental DTB tests from Santos et al. (2017)

		Case I	Case II	
Salt	-	$CaCO_3$	$BaSO_4$	-
Fluid density	ρ_β	934.8	975.45	kg/m³
Fluid dynamic viscosity	μ_β	$2.13x10^{-4}$	$3.81x10^{-4}$	Pa.s
Fluid flow rate	Q_β	10	10	mL/min
Solid particle density	ρ_p	2795	4500	kg/m³
Solid particle diameter	d_p	25	25	µm
Solid flow rate	$\dot{m}_P$	18.7	17.9	kg/m³/day
Adhesive force magnitude over particle weight	F_{adh}	$1x10^5$	$1x10^5$	-

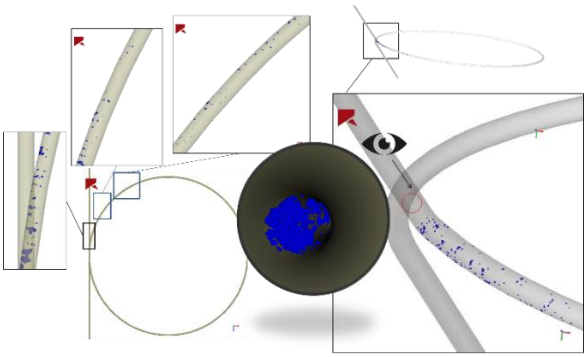

Figure 3. Scale formation at t=30 of case A in the DTB geometry, with inside view detail of the tube.

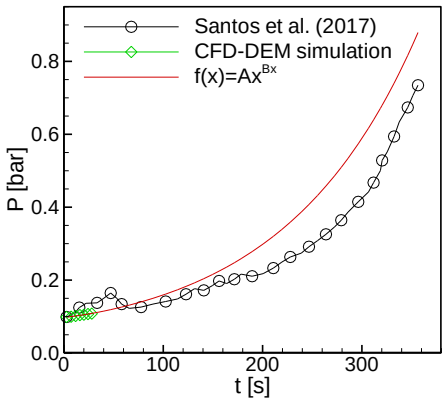

Figure 4. Extrapolation of the pressure differential obtained from case I simulation results at t=27 s and comparison with experimental results from Santos et al. (2017). A=9843; B=$1{,}05x10^{-3}$.

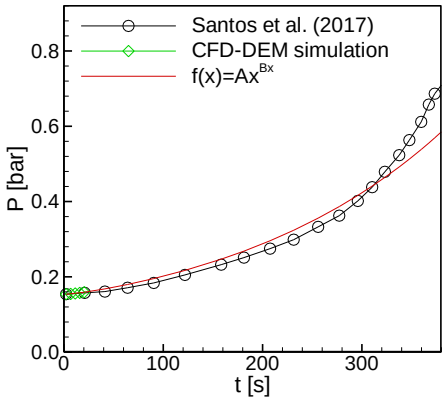

Figure 5. Extrapolation of the pressure differential obtained from case II simulation results at t=21 s and comparison with experimental results from Santos et al. (2017). A=15339; B=5,93x10^{-4}.

4. CFD-DEM VERIFICATION RESULTS: SSV MOCK-UP

The geometry of the SSV mock up is shown in Figure 6 (a) consisting of 16 ports with 32 mm diameter. Figure 6 (b) displays the fluid domain, with a exploded view shown in Figure 6 (c) comprising the annular region, the choke and the duct. The fluid inlets through the annular, accelerates through the choke and flow out the domain through the duct. production column. The particles are continuously injected near the trim (choke) entrance, following the fluid path. The simulation parameters are listed in Table 2, with water being used as fluid, and particle properties matching usual calcium carbonate crystals available in Martins et al. (2020).

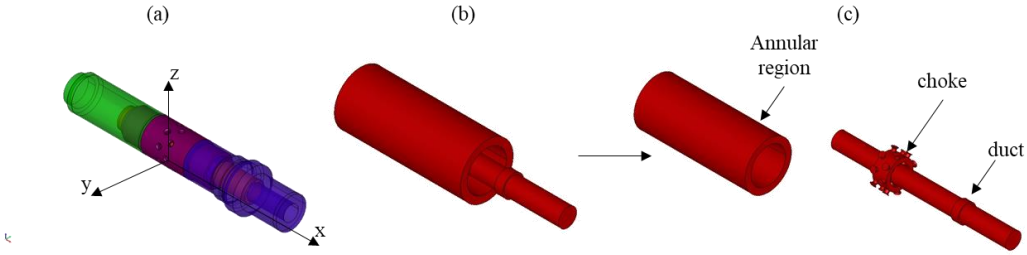

Figure 6. Schematic representation of the Sliding Sleeve Valve geometry: (a) valve mock up; (b) fluid domain; (c) exploded view of the fluid domain indicating the main parts.

Table 2. Simulation parameters for the CFD-DEM results.

Fluid density	ρ_β	1071	kg/m³
Fluid dynamic viscosity	μ_β	1.24x10^{-3}	Pa.s
Fluid flow rate at annular entrance 1	Q_β	14.4	m³/day
Fluid flow rate at annular entrance 2	Q_β	0	m³/day
Solid particle density	ρ_p	2795	kg/m³
Solid particle diameter	d_p	17.3	µm
Solid flow rate	$\dot{m}_P$	1.34x10^{-5}	kg/s
Young's modulus	E	10^8	N/m²
Particle-particle restitution coefficient	e	0.3	-
Particle-wall restitution coefficient	e	0.3	-
Static friction coefficient	μ_e	0.7	-
Dynamic friction coefficient	μ_d	0.7	-
Adhesive force magnitude	f_{adh}	1x10^4	-
Particle-particle adhesive force distance range	δ_{adh}	17.3	µm
Particle-wall adhesive force distance range	δ_{adh}	86.8	µm
Fluid time step	Δt_β	1x10^{-2}	s
Particle time step	Δt_p	1x10	s

Figure 7 displays the results for the CFD-DEM model on the SSV domain, with the white dots representing the particles. Solid agglomerates can be observed throughout the geometry, but are concentrated mostly near the trim region and on the ledge in the column. The accumulated mass is computed by the sum of all adhered particles and is plotted over time in Figure 8(a). The corresponding pressure curve in Figure 8(b) exhibits a linear uptrend for the 5 s simulated.

Both curves for pressure and mass were fitted to linear functions f(x)=Ax+B, as also used by Cheong et al. (2013) after similar extrapolation trends applied to erosion, to represent the data and estimate results at later times matching the 120-minute experimental time. Fits for the adhered mass and pressure returned good values of R^2. The predicted mass for t=2 h is 12.73 g, while the reference experimental results is approximately 2g. The extrapolated pressure peaked at 2.68 bar, while the experiment brings values within the range 0.3 to 0.4 bar. Indeed, it is not practical to reach a simulated time of 7200s with a time step listed in Table 2, also the particle time step is strict because of the major influence of the adhesion force. In fact, the scale formation is a non-linear phenomenon where there is a complex balance between adhesion and drag forces. As the fouling growths and the drag increases, is its easier for the fluid flow to wash away particles, yielding, therefore, a lower adhered mass and pressure. Such results will be pointed as the simulation keep running and more instants are obtained, elucidating the auto-cleaning effect imposed by the flow.

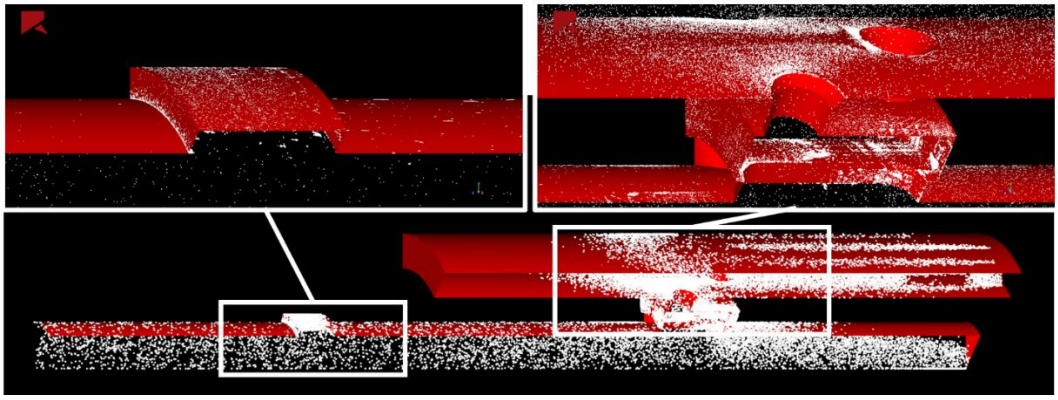

Figure 7. CFD-DEM results for particle adhesion on the SSV valve.

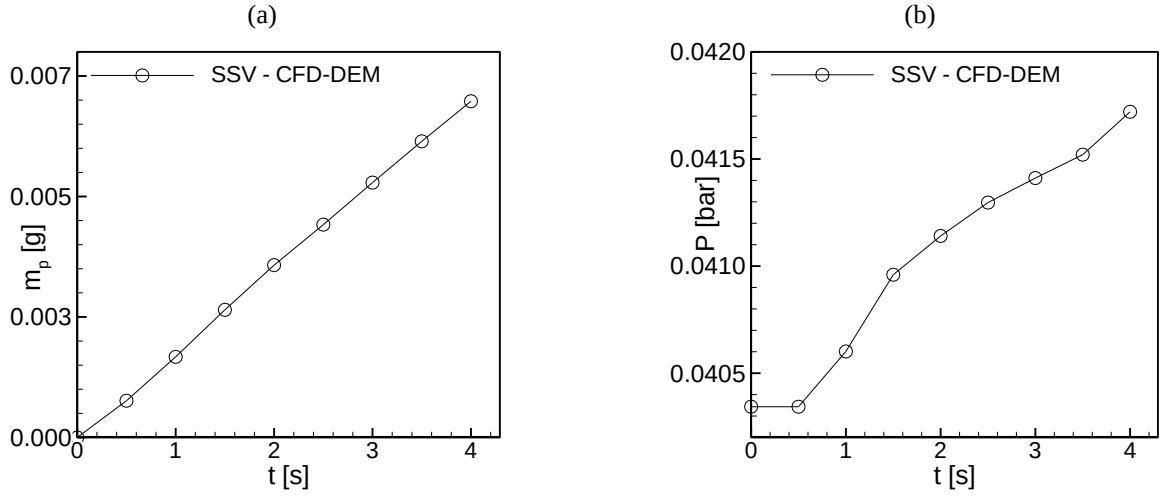

Curve fitting: m(x)=0,00177x-0,0000388 R^2=0.888
Extrapolation: m(2h) = 12,73 g

Curve fitting: p(x)=0,000366x+0,0403 R2=0.961
Extrapolation: p(2h) = 2,68 bar

Figure 8. CFD-DEM results for the numerical simulation of the scaling process in valves: (a) accumulated mass and (b) pressure increase, both as a function of time and the extrapolation function used to compute the total mass after 2h.

5. CONCLUSIONS

The present paper discusses the use of numerical simulation for the scaling tendency assessment in internal control valves. The employment of the Discrete Element Method accounted for the adhesive force, which led to agglomerates build up and particle adhesion on surfaces. The four-way-coupling scheme with the Finite Volume Method empowers the method with the possibility to include fluid dynamic effects over the particles. CFD-DEM is used to reproduce

experimental results obtained with a Dynamic Tube Blocking (DTB) experimental unit and a large-scale flow loop with a SSV mock assembled. Numerical results reproduced the pressure uptrend of the DTB correctly both in the simulated instants and in the extrapolated time. In the case of the SSV mock up, CFD-DEM resulted in values of extrapolated mass and pressure in the same order of magnitude of experimental results. Numerical results may be improved by further calibrating the adhesive forces and also extending the simulated time. Therefore, CFD-DEM is a robust method able to handle a turbulent flow with a population of millions of particles in a complex geometry, being suitable for the simulation of scale formation.

6. ACKNOWLEDGEMENTS

Authors are thankful for the support provided by CENPES/PETROBRAS, the Brazilian Petroleum Agency (ANP), the Human Resources Program for the Petroleum and Gas Sector PRH-ANP (PRH10-UTFPR), the UTFPR Science Foundation (FUNTEF-PR). Author also appreciate the partnership with the Engineering Simulation and Scientific Software (ESSS).

7. REFERENCES

Al-Anezi, K.; Johnson, D. J.;Hilal, N., 2008. “An atomic force miscroscope study of calcium carbonate adhesion to desalination process equipment: effect of anti-scale agent”. *Desalination*, V. 220, pp. 359-370.

Anderson, T. B.; Jackson, R., 1967. “A fluid mechanical description of fluidized beds - equations of motion”. *Industrial Chemical Engineering Fundamentals*, v. 6, n. 4, p. 527–539.

Cheong, W. C.; Gaskell, P. H.; Neville, A., 2013. “Substrate effect on surface adhesion/crystallisation of calcium carbonate”. *Journal of Crystal Growth*, V. 363, pp. 7-21.

Cosmo, R. P.; Pereira, F. A. R.; Soares, E. J.; Martins, A. L., 2022. “Modeling and validation of the CO_2 degassing effect on $CaCO_3$ precipitation using oilfield data”. *Fuel*. V.: 310, Part B.

Cundall, P. A.; Strack, O. D. L., 1979. “A Discrete Numerical Model for Granular Assemblies.” Géotechnique 29(1):47–65.

Ferreira, M. V. D.; Martins, A. L.; Maciel, R. S.; Fejoli, R. F.; Pereira, F. A. R.; Poletto, V. G.; De Lai, F. C.; Junqueira, S. L. M, 2020. "New Scale Prediction Approach Through Numerical Simulations." In: *SPE 2020 Annual Technical Conference and Exhibition*, Denver, Colorado, US.

Kokal, S., 2005. “Crude-Oil Emulsions: A State-Of-The-Art Review” In *2002 SPE Annual Technical Conference and Exhibition*, Santo Antonio, Texas, US.

Marshall, J. S. e Li, S. 2014 Adhesive Particle Flow – A Discrete-Element Approach. Cambridge University Press.

Martins, A. L.; Santos, H. F. L.; Castro, B. B.; Gonçalves, A. S.; Maffra, D. A.; Loureiro, J. B. R., 2020. “Large scale laboratory tests for calcium carbonate scaling in sliding sleeve valves” In *2020 SPE International Oilfield Scale Conference and Exhibition*, virtual.

Mores, M. H.; Poletto, V. G.; De Lai, F. C.; Junqueira, S. L. M, 2020. “Simulação numérica do escoamento em válvulas SSV”. In: *Rio Oil & Gas Expo and Conference 2020*, Rio de Janeiro, RJ, Brazil.

Morgan, V. G.; Sad, C. M. S.; Constantino, A. F.; Azeredo, R. B. V., Lacerda Jr, V.; Castro, E. V. R.; Barbosa, L. L., - 2019. “Droplet Size Distribution in Water-Crude Oil Emulsions by Low-Field NMR”. *Journal of the Brazilian Chemical Society*, V.: 30, N.: 8, pp.:1587-1598.

Morsi, S. A. e Alexander, A. J., 1972 “An investigation of particle trajectories in two-phase flow systems”. *Journal of Fluid Mechanics*, v. 55, n. 2, p. 193–208.

Peker, S.; Hevalce, S., 2008. “Solid-Liquid Two Phase Flow”. Elsevier Science.

Poletto, V. G.; De Lai, F. C.; Ferreira, M. V. D.; Martins, A. L., 2020. “Numerical Simulation to Study Scale Formation on SSV Valves” In *2020 SPE Oilfield Scale Conference and Exhibition*, virtual.

Popoff, B. and M. Braun. 2007. “A Lagrangian Approach to Dense Particulate Flow.” Pp. 510–21 in 6th International Conference on Multiphase Flow, ICMF 2007. Leipzig.

Santos, H. F. L.; Castro, B. B.; Martins, A. L.; Schlüter, H. E. P.; Júnior, M. F. S.; Jacinto, M. C.; Rosário, F. F., 2017. “A Physical Model for Scale Growth during the Dynamic Tube Blocking Test” In *2017 OTC Brasil*, Rio de Janeiro, RJ, Brazil.

Schnitzler, E.; Gonçalez, L. F.; Roman, R. S.; Marques, M.; Gutterres, F. R.; da Silva, M. F.; Castilho, C. A. B., 2021. "Buzios Presalt Wells: Delivering Intelligent Completion in Ultra-Deepwater Carbonate Reservoirs". In: SPE 2021 Offshore Technology Conference, Houston, Texas, US.

Shih, T.H.; Liou, W. W.; Shabbir, A.; Yang, Z.; Zhu, J., 1995. "A New - Eddy-Viscosity Model for High Reynolds Number Turbulent Flows - Model Development and Validation". *Computers Fluids*, 24(3), 227-238.

Silva, D. J.; Sorbie, K. S.; Mackay, E. J., 2018. "Introduction of Kinetic Effecs into the Thermodynamic Modelling of $CaCO_3$ Scale Precipitation" In *2018 SPE Oilfield Scale Conference and Exhibition*, Aberdeen, Scotland, UK.

Walton, O. R. e Braun, R. L. 1986. "Viscosity, granular-temperature, and stress calculations for shearing assemblies of inelastic, frictional disks" *Journal of Rheology*, vol. 30(5), pp.:949-980.